THE JOURNAL OF
PHYSICAL CHEMISTRY A

Article

pubs.acs.org/JPCA

Noise-Immune Cavity-Enhanced Optical Heterodyne Detection of HO_2 in the Near-Infrared Range

Claire L. Bell, Jean-Pierre H. van Helden, Tom P. J. Blaikie, Gus Hancock, Nicola J. van Leeuwen, Robert Peverall, and Grant A. D. Ritchie*

Physical & Theoretical Chemistry Laboratory, Department of Chemistry, University of Oxford, South Parks Road, Oxford OX1 3QZ, U.K.

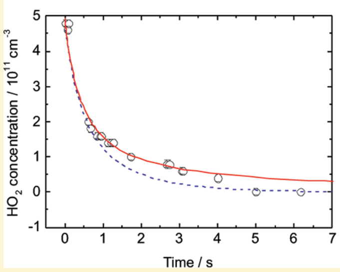

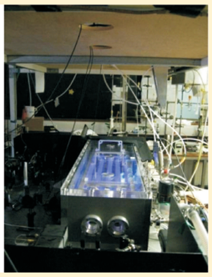

ABSTRACT: Accurate measurements of the absolute concentrations of radical species present in the atmosphere are invaluable for better understanding atmospheric processes and their impact on Earth systems. One of the most interesting species is HO_2, the hydroperoxyl radical, whose atmospheric daytime levels are on the order of 10 ppt and whose observation therefore requires very sensitive detection techniques. In this work, we demonstrate the first steps toward the application of external-cavity diode-laser-based noise-immune cavity-enhanced optical heterodyne molecular spectroscopy (NICE-OHMS) to the detection of the HO_2 radical in the near-infrared range. Measurements of stable species and of HO_2 were made in a laboratory setting, and the possibilities of extending the sensitivity of the technique to atmospheric conditions are discussed.

INTRODUCTION

The measurement of absolute concentrations of trace gases in the atmosphere has far-reaching implications, as such concentrations are crucial inputs for models that predict future air quality and climate change. The numerous, varied, and interlinked chemical cycles in the atmosphere are complex, and for models to be refined and improved, comparison with accurate data on the absolute concentrations of individual species constitutes the best validation. Field measurements therefore add tremendous value to theoretical modeling and have led to the development of increasingly effective measurement techniques.[1] When measuring trace gases, particularly in the field, in addition to achieving the necessary sensitivity, it is also highly desirable that any detection system be able to operate at ambient temperature and pressure and without the need for extensive sample preparation. It is also an important requirement that absolute concentrations of species can be obtained.

Radical species, such as OH and HO_2, control virtually all of the daytime oxidative chemistry in the lower atmosphere and are responsible for the transformation of primary emissions into secondary pollutants.[2] Important climate gases such as methane and ozone are also intricately related to the concentration of HO_2; their atmospheric lifetimes depend on the concentration of HO_2, which also controls the production of acidic species, with their well-known detrimental effects to the environment. Although undoubtedly important, HO_2 provides a range of challenges when considering appropriate detection techniques as atmospheric daytime levels of HO_2 are very small [$\sim 2.5 \times 10^8$ molecules cm^{-3} $\equiv$ 10 parts per trillion (ppt)] and so require very sensitive detection techniques. Currently, HO_2 is measured by the indirect techniques FAGE (fluorescence assay by gas expansion), which is essentially laser-induced fluorescence at low pressure,[2−8] and PERCA (peroxy radical chain amplification), whereby HO_2 and RO_2 catalyze the oxidation of NO and CO into CO_2 and NO_2, which can then be measured.[9−13] Although FAGE specifically measures HO_2 (indirectly through its conversion into OH), it suffers from interference from RO_2 radicals.[14] PERCA traditionally measures the sum of all RO_2 species, although we note that a very recent work showed the possibility of selective measurement of atmospheric peroxy radical concentrations of HO_2 and RO_2 using a denuding method based on PERCA.[15] It is therefore desirable to have a direct and speciated technique.

A highly attractive analytical method for trace gas sensing that offers the required selectivity, can return absolute number densities, and might have the required sensitivity levels is absorption spectroscopy. In the ultraviolet (UV) range, where optical techniques traditionally operate, the spectroscopy of HO_2 has been extensively studied, and important information on reaction kinetics has been acquired in laboratory experiments.[16−22] Although the cross sections for electronic excitation of HO_2 are large ($\sigma = 10^{-18}$ cm^2), the absorption spectrum of HO_2 is broad and structureless, and there is interference from other species, such as other peroxy radicals and hydrogen peroxide, the main product of HO_2 self-reaction. The commercial development of diode lasers in the near-infrared range opened up the opportunity of studying HO_2 in this range, and subsequent investigations into these narrower and better-resolved absorption features and their use in

Received: February 1, 2012
Revised: April 18, 2012
Published: May 16, 2012

dx.doi.org/10.1021/jp301038r | J. Phys. Chem. A 2012, 116, 5090−5099

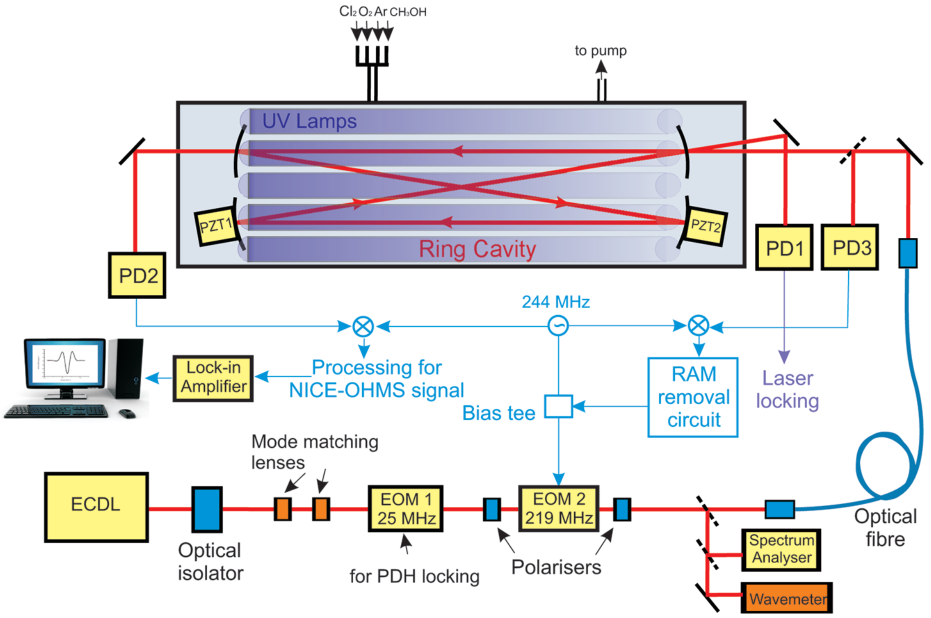

Figure 1. Experimental setup for the NICE-OHMS experiments detailing the ring cavity and a schematic diagram of the electronics. ECDL, external cavity diode laser; EOM, electro-optic modulator; PD1, PD2, and PD3, photodiodes 1, 2, and 3, respectively; PZT1 and PZT2, piezoelectric transducers.

studying HO_2 kinetics have been published.[23−37] The HO_2 absorption bands in the near-infrared range are a vibronic progression in the low-lying $^2A' \leftarrow {}^2A''$ electronic transition ($\sim$7017 cm^{-1}), along with the first vibrational overtone in the OH stretch ($2\nu_1$) centered at 6649 cm^{-1}. It is this latter band that we probe in this work, because, although the spectral range offers smaller line strengths than the mid-infrared and UV ranges,[38,39] it does offer advantages through the availability of cheap, commercially available continuous-wave (cw) laser sources such as the external-cavity diode laser (ECDL) (1480−1540 nm) used in this work. The commercial importance of diode lasers in the telecommunications and consumer electronics industries drives their ongoing development, resulting in lasers being available at a wide range of wavelengths (375−430 and 630−2700 nm) with suitable powers and narrow linewidths. The introduction of cw quantum cascade lasers in the past decade has now enabled expansion into the mid-infrared range as has been recently reported for HO_2 probing the ν_3 band, which has absorption cross sections 1 order of magnitude larger than in the near-infrared range.[40,41]

Previous works have reported a variety of diode-laser-based experiments in the near-infrared range within the $2\nu_1$ band to detect HO_2, including Taatjes and Oh using wavelength-modulation spectroscopy (WMS)[25] and DeSain et al. using two-tone frequency-modulation spectroscopy (TTFMS) to measure the line positions with high resolution.[26] In most of these studies, heterodyne detection techniques such as WMS and TTFMS were used to measure small absorbances, often in combination with multipass cells, such as Herriott-type flow cells, to increase the absorption path length. In studies by Ibrahim et al. on air-broadening coefficients[34] and by Thiebaud et al. on detailed high-resolution measurements of absorption cross sections,[35] continuous-wave cavity ring-down spectroscopy (cw-CRDS) was used to monitor time-resolved HO_2 concentrations. With this technique, a detection limit for HO_2 of 3.2×10^9 cm^{-3} for a 1 Hz detection bandwidth was obtained at a pressure of 25 Torr.[42] In this method, light is trapped in a high-finesse optical resonator consisting of two highly reflective mirrors containing the sample under investigation and undergoes repeated reflections such that the effective optical path length is on the order a few kilometers in a tabletop setup. Although the basic technique of cw-CRDS is well-established and has been confirmed to be one of the most convenient and useful sensitive spectroscopic methods regularly reaching sensitivities on the order of 10^{-9} cm^{-1},[43] it is insufficient for the purpose of HO_2 detection under atmospheric conditions, which requires an absorption coefficient of $\sim 10^{-12}$ cm^{-1} to be measured; for reliable quantification, even an order of magnitude lower would be needed. The true potential of optical cavity-based cw laser absorption spectroscopy is realized, however, when the radiation is coupled into an optical cavity that is locked in resonance with the laser wavelength. There are multiple advantages in conducting spectroscopy within fully resonant cavities, including increased power levels on the detectors, which lead to a reduction in the shot-noise limit; excitation of single stable cavity modes, which leads to a narrower distribution of ring-down times; and increased data acquisition rates. Sensitivities on the order of 10^{-11}−10^{-12} cm^{-1} $Hz^{-1/2}$ are expected and, indeed, have been attained in a handful of elegant experimental methods.[43]

However, where truly ultrasensitive detection is required, as is the case for the atmospheric detection of HO_2, the potential that the noise-immune cavity-enhanced optical heterodyne molecular spectroscopy (NICE-OHMS) technique offers is unrivalled. Pioneered by Ye and Hall,[44] this technique requires that the laser be locked on resonance with the cavity, utilizing the increase in path length and signal, while also frequency modulating the input radiation. In *fm*-NICE-OHMS, a specific case of frequency-modulation spectroscopy (FMS) is performed in which the modulation frequency is carefully selected to exactly match that of the cavity free spectral range or multiples thereof. This leads to the “noise-immunity” feature of

NICE-OHMS; as the frequency components of the FM triplet (carrier frequency and sidebands) are all separated by the free spectral range, each is transmitted through the cavity in the same way (i.e., maintaining the resonance with a cavity mode), with each component being affected identically by the cavity. As the *fm*-NICE-OHMS signal arises from the beating between the carrier and the sidebands, the signal is noise-immune to jitter in the laser frequency, which is responsible for most of the sensitivity-limiting noise in the signal. The use of modulation techniques transposes the signal to high frequency (a few hundred megahertz) to achieve a reduction in the noise. On top of this, a "slower" wavelength-modulation spectroscopy (WMS) can be applied to further improve the sensitivity (*wm*-NICE-OHMS), for example, by altering a piezoelectric transducer on one of the cavity mirrors.

Although NICE-OHMS has yielded unprecedented sensitivities of 10^{-14} cm^{-1} $Hz^{-1/2}$, we note that such performance has been observed only in measurements of sub-Doppler saturated line shapes.[45] Other practitioners have shown that the technique becomes limited by noise associated with etalon structures that become evident only when scanning over hundreds of megahertz, as is generally necessary for making observations of molecular species.[46−48] For example, the Axner group used fiber-laser-based NICE-OHMS for Doppler-broadened detection of C_2H_2 and CO_2 around 1531 nm using a cavity with a finesse of 4800 with a minimum detectable absorption of 3.5×10^{-11} cm^{-1} $Hz^{-1/2}$[47] and most recently reported a sensitivity of 1.8×10^{-11} cm^{-1} $Hz^{-1/2}$.[49] We recently reported the performance of an ECDL-based NICE-OHMS spectrometer and obtained a sensitivity of 4×10^{-11} cm^{-1} $Hz^{-1/2}$.[50] In this article, we present the application of this near-infrared NICE-OHMS spectrometer to the detection of the HO_2 radical. Spectra from stable species of atmospheric relevance, namely, CO_2, CH_4, and N_2O, are used to illustrate the performance of the spectrometer and to demonstrate that the technique is capable of measuring spectral parameters. We then present the first application of the NICE-OHMS system as an accurate and direct technique for measuring the concentration of the hydroperoxyl radical HO_2 in a laboratory setting.

■ EXPERIMENTAL DETAILS

Optical Setup. A schematic of the experimental setup is shown in Figure 1. The light source was an ECDL (Sacher Lasertechnik LION, linewidth < 2 MHz) tunable in the range of 1480−1540 nm with a maximum output power of 3.2 mW providing a mode-hop free tuning range of 56 GHz using current coupling. The laser light was first directed through an optical isolator (Isowave I-15-UHP-4 1550 nm) to prevent optical feedback before passing through two beam-shaping lenses, which reshaped the elliptical beam output from the laser to a predominantly Gaussian-shaped beam, mimicking the TEM_{00} mode of the cavity. Two electro-optic modulators (EOMs) were situated after these lenses: EOM1 [Nova phase electro-optic phase modulator (EO-PM-NR-C3)] to modulate the light for locking the laser frequency to a TEM_{00} mode of the cavity and EOM2 [Quantum Technologies (TWAP 10-1350-1650 nm)] for modulation at the cavity free spectral range and, hence, postcavity FM detection. To isolate the alignment of the beam into the cavity from adjustments to the laser and EOMs and also to provide a clean, predominantly Gaussian-shaped beam, the light was fed through a single-mode polarization preserving fiber (OZ Optics). The resulting power incident on the cavity was 1 mW. The wavelength of the laser was monitored with a wavemeter (Burleigh WA-1000), and a frequency scale for the data was defined by monitoring the laser output with a spectrum analyzer (10 GHz Melles Griot 1300−1500 nm, adjusted for 0.81 GHz free spectral range).

The ring cavity was formed by four high-reflectivity mirrors (1 in. in diameter, radius of curvature of $r = -1$ m) in a bow-tie configuration with a half-round trip length, L, of 137 cm and a cavity free spectral range (FSR) of 109.5 MHz. The specified reflectivity of the input and output coupling mirrors was 0.9994 (Newport 10CV00SR.70T), and that of the other two mirrors was 0.9997 (Newport 10CV00SR.70F). The two highest-reflectivity mirrors were mounted on piezoelectric transducers (PZTs): PZT1 (PiezoMechanik HPSt 150/20-15/55) was used for scanning the cavity length, and PZT2 (Physik Instrumente GmbH P-622.10 L) was used for the modulation of the cavity length for WMS. The vacuum chamber housing the ring cavity was evacuated to 10^{-4} Torr before it was filled with a given pressure of gas, monitored with a capacitance manometer (MKS instruments 722A11TBA2FA, 0−10 Torr). To avoid etalons, wedged windows (antireflection coated for 1050−1600 nm) were used on the vacuum chamber.

Electronic Components. The electronic components were numerous and finely tuned to the power and frequency of the laser source. For the locking of the laser frequency to a cavity TEM_{00} mode and the FM frequency to twice the cavity FSR, three frequencies were generated by two voltage-controlled oscillators (VCOs, Mini-Circuits JTOS-300). Signals were generated at 219 and 244 MHz (used for the FSR locking) and mixed and filtered to produce the 25 MHz difference frequency used for locking the laser to the cavity. The laser frequency was locked to a TEM_{00} mode of the cavity using the Pound−Drever−Hall (PDH) method,[51] with EOM1 used to produce sidebands at ±25 MHz on the laser frequency. The laser light reflected from the cavity was directed onto a fast photodetector (PD1) (New Focus 1611) with a bandwidth of 1 GHz, amplified (Mini-Circuits ZFL-500LN), and then demodulated at 25 MHz using a double balance mixer (Mini-Circuits ZAD-1) to generate the PDH error signal. This error signal was processed by a fast (megahertz) locking circuit with a bandwidth of ~2 MHz and fed back to the laser injection current for primary locking of the laser frequency to the cavity. With the laser locked to the cavity, the cavity length was changed such that the laser frequency was scanned over a preselected range by applying a sinusoidal voltage ramp, at a frequency of 1 Hz, to PZT1. A slow locking circuit followed the change in cavity length and generated a signal that was fed back to the laser PZT input for the ECDL, to maintain the lock of the laser to the cavity while scanning the cavity length. The bandwidth of the laser when locked was necessarily less than ~50 kHz. A feed-forward loop was implemented in the locking scheme to reduce the load placed on the locking electronics and to increase the scan rate for which mode-hop free tuning of the laser was maintained.

To perform *fm*-NICE-OHMS, EOM2 frequency-modulated the laser light at ~219 MHz to generate sidebands at ±2 times the FSR from the carrier laser frequency. However, the FSR of the cavity changes slightly during a frequency scan over an absorption line as the length of the cavity changes, and the noise-immune aspect of NICE-OHMS requires a good match between the modulation frequency and the FSR of the cavity. Hence, the modulation frequency was locked to the FSR using

Table 1. Reactions Occurring during HO_2 Generation and Their Corresponding Rate Constants

	reaction	rate constant	units	ref
R1	$Cl_2 \rightarrow Cl + Cl$	7×10^{-3}	s^{-1}	this work
R2	$Cl + CH_3OH \rightarrow CH_2OH + HCl$	5.5×10^{-11}	cm^3 $molecule^{-1}$ s^{-1}	53
R3	$CH_2OH + O_2 \rightarrow HO_2 + H_2CO$	9.1×10^{-12}	cm^3 $molecule^{-1}$ s^{-1}	53
R4	$HO_2 + Cl \rightarrow HCl + O_2$	3.5×10^{-11}	cm^3 $molecule^{-1}$ s^{-1}	53
R5	$HO_2 + Cl \rightarrow OH + ClO$	1.0×10^{-11}	cm^3 $molecule^{-1}$ s^{-1}	53
R6	$HO_2 + CH_2OH \rightarrow H_2CO + H_2O_2$	2.0×10^{-11}	cm^3 $molecule^{-1}$ s^{-1}	54
R7	$HO_2 + HO_2 \rightarrow H_2O_2 + O_2$	1.4×10^{-12}	cm^3 $molecule^{-1}$ s^{-1}	53
R8	$Cl + CH_2OH \rightarrow H_2CO + HCl$	6.6×10^{-10}	cm^3 $molecule^{-1}$ s^{-1}	55
R9	$H_2O_2 + Cl \rightarrow HCl + HO_2$	4.1×10^{-13}	cm^3 $molecule^{-1}$ s^{-1}	53
R10	$OH + H_2O_2 \rightarrow HO_2 + H_2O$	1.8×10^{-12}	cm^3 $molecule^{-1}$ s^{-1}	53
R11	$H_2CO + Cl \rightarrow HCO + HCl$	7.3×10^{-11}	cm^3 $molecule^{-1}$ s^{-1}	53
R12	$CH_2OH + Cl_2 \rightarrow ClCH_2OH + Cl$	2.9×10^{-11}	cm^3 $molecule^{-1}$ s^{-1}	56

the DeVoe and Brewer method:[52] A fraction of the amplified signal from PD1 was split off (Mini-Circuits ZFSC-2-1-S) and demodulated with a double balance mixer (Mini-Circuits ZAD-1) at 244 MHz (the sum of the cavity FSR and the PDH locking frequency) to produce an error signal for locking the FM frequency to the cavity FSR. This error signal was fed into a proportional−integral locking circuit to adjust the tuning voltage on the VCO and thus the modulation frequency of EOM2 to match twice the FSR.

To produce the *fm*-NICE-OHMS signal, the ac output of a second photodetector PD2 (New Focus 1611) was amplified (Mini-Circuits ZKl-1R5 and ZFL500HLN) and high-pass-filtered (Mini-Circuits SHP-175), before being demodulated at ∼219 MHz with a double balance mixer (Mini-Circuits ZDM-1W-S). This signal was passed through a 100 Hz low-pass filter, recorded using a digital oscilloscope (Lecroy 9304), and stored on a computer. Changing the demodulation phase allowed either the absorption or dispersion FMS signal to be acquired. Following the generation of the *fm*-NICE-OHMS signal, the detection sensitivity can be further improved by applying an additional modulation to the cavity in the form of WMS. The cavity length and, through the locking circuit, the laser frequency were dithered using PZT2 at a low frequency of 60 Hz with a frequency excursion of 0.1 GHz. To produce this *wm*-NICE-OHMS signal, the *fm*-NICE-OHMS signal was demodulated at 60 Hz using a lock-in amplifier (EG&G 7265 DSP). Demodulation of the signal occurred with a time constant of 50 ms, corresponding to a bandwidth of 3.2 Hz. Again, the processed signals were recorded with the oscilloscope and passed to a computer for analysis.

The maximum sensitivity that could be achieved was limited by residual amplitude modulation (RAM) resulting from imperfections in the EOMs and etalons before the cavity, whereby some of the radio frequency applied through the EOM induces amplitude modulation, leading to undesirable noise on the detected signal. Etalon effects were minimized with the use of wedged windows, careful alignment of the optical components, and using optical fibres with angled ends. A simple method of removing a background variation would be to implement a background subtraction technique, whereby the signals are taken both with and without the absorber present in the cavity and then subtracted from one another to remove the background variation. However, this approach was not possible with this NICE-OHMS setup, given the drift in the laser, and the necessity to maintain the laser lock to the cavity over the entire data acquisition period.

HO_2 Generation and Kinetic Modeling. HO_2 was generated within the optical cavity through Cl-atom reactions with CH_3OH and O_2, which were initiated by the continuous-wave photolysis of Cl_2 by UV lamps

$$Cl_2 + h\nu \rightarrow Cl + Cl \tag{1}$$

$$Cl + CH_3OH \rightarrow CH_2OH + HCl \tag{2}$$

$$CH_2OH + O_2 \rightarrow HO_2 + H_2CO \tag{3}$$

A more complete reaction scheme, including all of the major reactions involved in the generation and loss of HO_2 with their rate constants, is listed in Table 1. Detailed modeling of the HO_2 production and reaction scheme was undertaken to predict the concentrations of HO_2 and of potentially interfering species that also absorb around 1.5 μm, such as H_2CO. For the modeling, an estimate of the rate constant for Cl_2 photolysis was needed (reaction 1) for our particular experimental configuration.

To photolyze Cl_2, five UV lamps were fitted in the top of the vacuum chamber, 2 cm above the bow-tie cavity, beneath the Perspex lid. The spectrum of one of the lamps (Philips Sylvania TLD F18W black light blue tubes) was recorded using a Jobin Yvon spectrometer (CP200), and in combination with knowledge of the power of one lamp (18 W), this allowed the number of photons emitted (per nanometer per second) to be calculated. Considering the five-lamp configuration inside the vacuum housing and the assumption that one-fourth of the radiation from each lamp was incident on the sample based on the geometry of the vacuum chamber, the flux of photons, $I_0(\lambda)$ (cm^{-2} s^{-1}), was thus estimated at 2 cm below the lamps, that is, at the beam path in the cavity. In the case of weak absorption, as here, the Beer−Lambert law can be applied to calculate the number of photons absorbed in 1 cm^{-3} in 1 s

$$I_{abs}(\lambda) = I_0(\lambda)\varepsilon(\lambda)cl \tag{4}$$

where $\varepsilon(\lambda)$ is the wavelength-dependent absorption cross section of chlorine; c is the concentration of Cl_2; and l is the interaction length, taken to be 1 cm. Integrating this expression over the wavelength range of interest results in the number of photons absorbed per cubic centimeter per second, which corresponds to the rate of Cl_2 dissociated (assuming that the quantum yield for photodissociation is unity). The rate constant for chlorine-atom production, k, is defined as $d[Cl]/dt = k[Cl_2]$ and is therefore equal to $2\int_0^\infty I_0(\lambda)\ \varepsilon(\lambda)\ d\lambda$; this gives a rate constant for these experimental conditions of $7 \times 10^{-3}\ s^{-1}$. For a similar experiment, the rate constant for chlorine-atom production was measured as $1.35 \times 10^{-3}\ s^{-1}$ for one lamp,[57] corresponding to a value of $6.7 \times 10^{-3}\ s^{-1}$ if five lamps were used. We note that the value determined here, which uses the assumption that a geometrical factor of one-fourth of the photons emitted interact with Cl_2, does not control the HO_2 concentration; modeling with the photolysis rate constant increased by a factor of four led to the HO_2 concentration increasing by only 1%, because both the production and loss rates of HO_2 are mainly dependent on species formed through photolysis.

The HO_2 peak absorption cross sections in the 1.5-μm range are typically around $\sigma = 1 \times 10^{-19}\ cm^2$,[35] and to ensure that detection of HO_2 was successful and well within the capabilities of the NICE-OHMS spectrometer, an initial minimal absorption coefficient, α_{min}, of $10^{-7}\ cm^{-1}$ was determined. The required concentration of HO_2 molecules was $\sim 8 \times 10^{11}$ molecules cm^{-3}, and kinetic modeling was undertaken, with initial concentrations of reactants chosen to generate HO_2 at this concentration. The simulation models continuously flowing products and reactants, with the entire gas volume in the vacuum chamber (36800 cm^3) being replaced every 120 s. Simulations were performed with and without wall-loss processes, with the effective rate constants estimated using the method of Chantry,[58] and their effects are discussed later.

The steel and Perspex vacuum assembly housing the ring cavity was first evacuated to 10^{-4} Torr before being filled to 760 Torr with N_2. After the lights had been switched on, the chamber was evacuated to a pressure of 40 Torr, and the flows of constituent gases were started. Flows of 18.2 sccm (standard cubic centimeters per minute) of 1% Cl_2 in Ar (certified purity of 1.00% in argon balance), 3.7 sccm of O_2 (BOC, certified purity of 99.5%), and 1719 sccm of Ar (BOC Pureshield, 99.998% purity) were controlled by mass flow controllers (Tylan FC-260), with the flow of 1.83 sccm of CH_3OH vapor being controlled through a calibrated needle valve. Pressures inside the vacuum chamber were measured with two capacitance manometers (MKS Instruments, 0−100 and 0−760 Torr), with the total pressure in the cell of reactants and buffer gas being controlled actively with a valve in the exit path before the pump. With the flows and lamps on, the locking procedure was implemented, as outlined above.

■ RESULTS AND DISCUSSION

Spectrometer Characterization. In this section, observations of a selection of weak transitions of methane, carbon dioxide, and nitrous oxide across 52 cm^{-1} (from 6595 to 6647 cm^{-1}) are presented, demonstrating (i) the calibration of the technique, (ii) the broad operating range of the spectrometer, and (iii) its applicability for returning spectroscopic parameters such as pressure-broadening parameters.

Locked CEAS. Calibration of the spectrometer requires the finesse of the optical cavity to be determined. To this end, the transmission of the cavity was monitored by a fast photodetector (PD2), and its dc output recorded in a locked cavity-enhanced absorption spectroscopy (CEAS) experiment with the same data acquisition system but with the electronics for *fm*-NICE-OHMS switched off. For CEAS, the transmission through the cavity can be represented by the modified Beer−Lambert law

$$\frac{I_0(\nu) - I(\nu)}{I(\nu)} = \frac{\alpha(\nu)L}{1 - R} \tag{5}$$

where $I(\nu)$ and $I_0(\nu)$ are the transmitted intensities with and without an absorbing species present, respectively; $\alpha(\nu)$ is the frequency-dependent absorption coefficient (the product of the absorption cross section and the absorber number density); L is the cavity length; and R is the geometric mean of the mirror reflectivity.[43]

For the determination of the cavity finesse, 25 Torr of methane was introduced into the cavity, and the CEA spectrum was recorded for an unassigned and weak CH_4 transition at 6595.90 cm^{-1} with an integrated absorption cross section, σ_{int}, of $1.115 \times 10^{-25}\ cm^2\ cm^{-1}$ obtained from the HITRAN database.[59] Recent high-resolution CRDS measurements by Campargue et al.[60] gave very similar results for the line strengths. Figure 2 shows a typical locked CEAS trace for 25 Torr of CH_4 along with a Voigt fit with the Gaussian component fixed to the calculated full width at half-maximum (fwhm) Doppler width of 611 MHz appropriate for a sample at 298 K. This CEA spectrum was acquired by scanning over 5 GHz at a scan rate of 1 Hz; the signal was acquired with 30 averages over an acquisition time of 30 s. The returned Lorentzian component of the fit was 91 ± 3 MHz (fwhm), which does not agree well with the calculated value for self-broadening of 138 MHz using the self-broadening parameter reported in the HITRAN database for transitions in this range.[59] However, widespread values are reported in the literature for the self-broadening of CH_4 transitions in various vibrational bands,[61,62] and our value is within these limits. A mean mirror reflectivity R of 0.9985 ± 0.0001, and thus a finesse of 2100 ± 200, was calculated from the integrated area, A, of the locked CEAS data, and the determined sensitivity was $6.5 \times 10^{-8}\ cm^{-1}$. The moderate sensitivity is partly due to the fact that, in locked CEAS, any phase and frequency modulations are converted into residual amplitude modulation, which increases the noise on the signal; the NICE-OHMS technique seeks to minimize these effects by utilizing modulation spectroscopy within a fully resonant cavity.

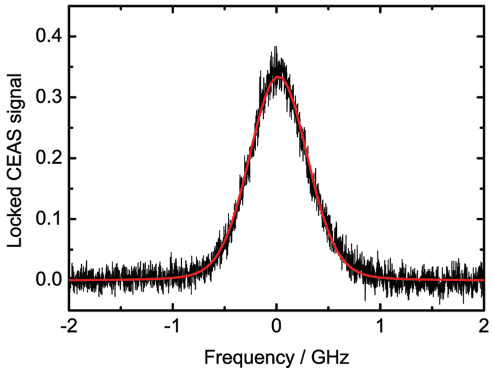

Figure 2. Typical locked CEAS spectrum of 25 Torr of CH_4 at 6595.90 cm^{-1}.

Broad Wavelength Tunability and Pressure Broadening. To analyze the performance of the spectrometer over a broad wavelength range and to demonstrate that the technique is capable of measuring spectral parameters, this section details observations on CO_2 measurements and the measurement of pressure-broadening parameters for CH_4 and N_2O. Figure 3 shows *fm*- and *wm*-NICE-OHMS signals for the P34(e) transition in the $\nu_1 + \nu_2 + 2\nu_3$ band of CO_2 at 6646.58 cm^{-1} with the highest sensitivity achieved with this measurement being 2×10^{-10} cm^{-1}. This is 2 orders of magnitude improvement in the sensitivity over locked CEAS. The signal was acquired with six averages over an acquisition time of 10 s. We found that this was the optimal acquisition time to provide the maximum signal-to-noise ratio, limited by longer-term laser drift problems. It should be emphasized that the position of the CO_2 transition is 40 cm^{-1} from the spectral position where CH_4 data were taken previously, which resulted in a sensitivity of 3×10^{-11} cm^{-1} for *wm*-NICE-OHMS.[50] The response of the laser to the locking is not constant across the broad spectral range accessible with the laser, resulting in a varying amplitude modulation across the spectral range and a different level of noise. The highest sensitivities achieved with the system occur in the spectral range around 6596 cm^{-1}, for which the system was initially designed and optimized. From measurements across the tuning range of the laser, it is clear that optimizing the electronics at each spectral range is particularly important and can markedly improve the sensitivity attained; yet this is time-consuming and often not possible when designing a field instrument for practical application. However, despite this variation in sensitivity across wavelength ranges, we note that the ability to apply NICE-OHMS to various transitions across different ranges of the spectrum while still achieving sensitivities of around 10^{-10} cm^{-1} is of great benefit when designing a spectrometer that can meet a wide range of detection requirements.

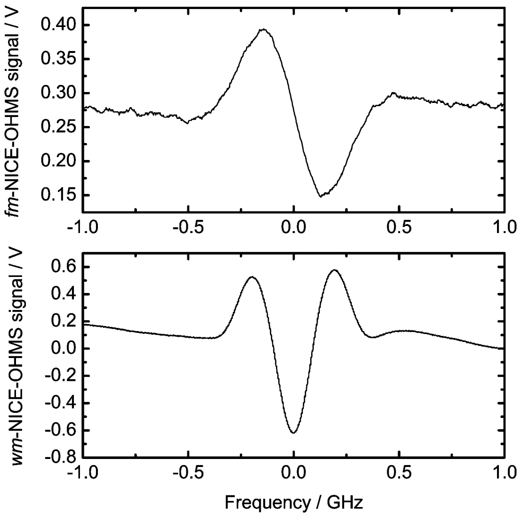

Figure 3. *fm*- and *wm*-NICE-OHMS signals for the P34(e) transition in the $\nu_1 + \nu_2 + 2\nu_3$ band at 6646.58 cm^{-1} for 8.1 (*fm*-NICE-OHMS) and 0.2 Torr (*wm*-NICE-OHMS) of CO_2.

To verify the linearity of the technique, the relationship between the amplitude of the absorption feature and the pressure of added gas was recorded for both the *fm*-NICE-OHMS and *wm*-NICE-OHMS signals with increasing pressures of CO_2. In both cases, the amplitudes increased linearly with increasing pressure of gas, with the results being shown in Figure 4. The nonzero intercept gives an indication of the noise inherent in the measurements and will determine the minimal sensitivity achievable with the system. *fm*-NICE-OHMS was then used to determine pressure-broadening coefficients for the unassigned transition of CH_4 at 6610.06 cm^{-1} broadened by helium. Twenty-five Torr of CH_4 was added to the evacuated cavity, after which increasing amounts of He were added, from 2 to 300 Torr. At each pressure, *fm*-NICE-OHMS data were recorded at both the absorption and dispersion phases. The FM data were fitted using a Voigt profile, fixing the fwhm of the Gaussian component of the fit to the theoretical value of 611 MHz and allowing the half-width at half-maximum (hwhm) of the Lorentzian component of the fit to vary. From this fitting routine, the Lorentzian width of each absorption profile was obtained. As demonstrated by the typical trace showing the data (black line) and fit (red line) in Figure 5, the signals of both the absorption (top) and dispersion (bottom) phases for 25 Torr of CH_4 broadened by 150 Torr of helium are well-represented by Voigt profiles transformed into FM space. During the data acquisition routine, only one phase of the data (absorption or dispersion) can be acquired per scan, with the operator selecting the phase. Hence, for the data presented here, at each pressure, both the absorption and dispersion signals were acquired separately, but during the same lock. The time delay between each pair of measurements was around 20 s. In Figure 6, the Lorentzian component of each fit from the absorption spectra is plotted against pressure, with a straight line fitted to the points. From the graph, a pressure-broadening coefficient of 1.5 ± 0.1 MHz $Torr^{-1}$ (hwhm) is obtained, which corresponds well with the literature values of 1.3−1.7 MHz $Torr^{-1}$ for transitions within the $2\nu_3$ band of methane at 1.65 μm.[63,64] The figure shows again a *y*-axis offset of 44 ± 5 MHz attributable to self-broadening that is consistent with the locked CEAS experiment for 25 Torr of pure CH_4.

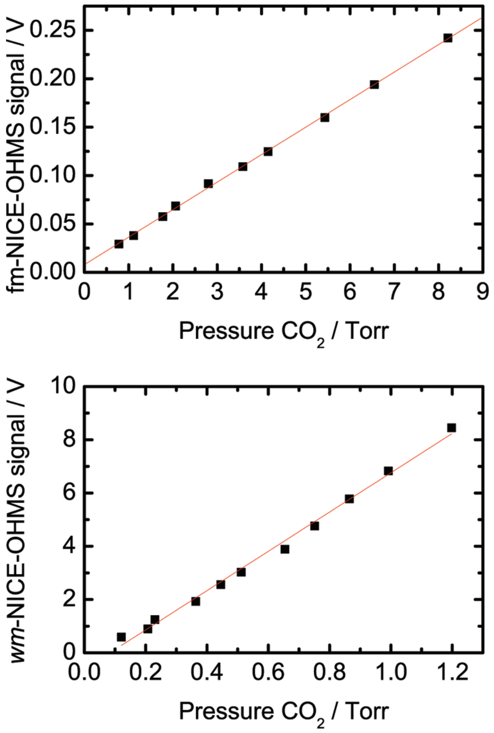

Figure 4. Plots of signal height versus pressure of CO_2 gas for *fm*-NICE-OHMS and *wm*-NICE-OHMS data.

A similar procedure was undertaken to retrieve pressure-broadening coefficients of N_2O broadened by the addition of helium. Figure 7 shows the *fm*-NICE-OHMS absorption signal

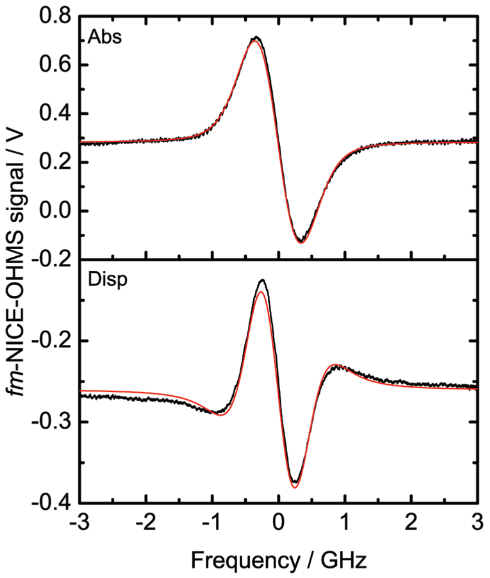

Figure 5. Simultaneous fitting for the (top) absorption and (bottom) dispersion spectra of 25 Torr of CH_4 at 6610.063 cm^{-1} broadened by 150 Torr of helium.

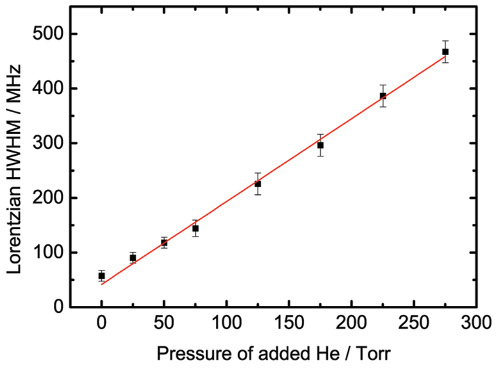

Figure 6. Lorentzian hwhm from the absorption spectra as a function of pressure for 25 Torr of CH_4 broadened by He.

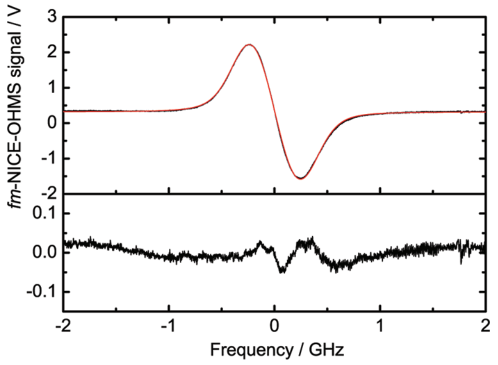

Figure 7. Typical absorption *fm*-NICE-OHMS signal of 0.42 Torr of N_2O in 50 Torr of He, with a fit to the data and the associated residuals plot.

(black) with the corresponding fit (red) for 0.42 Torr of N_2O broadened by 50 Torr of helium for the R28(e) transition in the ν_3 band. For the signals broadened by helium, again each absorption-based *fm*-NICE-OHMS trace was fitted with the Gaussian width fixed to the calculated value of 366 MHz, and the Lorentzian component of the Voigt profile was allowed to vary. Figure 8 shows the plot of the Lorentzian hwhm component of each fit against pressure, with a straight line yielding a pressure-broadening coefficient of 2.2 ± 0.1 MHz $Torr^{-1}$, in excellent agreement with the literature value of 2.1 MHz $Torr^{-1}$ for the P(26) transition in the same ν_3 band.[65]

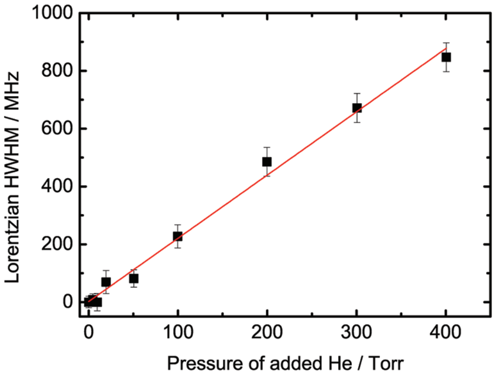

Figure 8. Lorentzian hwhm as a function of pressure for 0.42 Torr of N_2O broadened by He.

Spectroscopic Detection of HO_2. Having shown the calibration and broad wavelength tunability of our NICE-OHMS spectrometer with stable species, the final part of this article focuses on the detection of the hydroperoxyl radical HO_2 in a laboratory setting. Specifically, the near-infrared radiation of the laser probes the first vibrational overtone in the OH stretch, $2\nu_1$ (centered at 6648.9 cm^{-1}). The two absorption features selected for investigation in this work were assigned by DeSain et al.[26] as the ${}^{q}P_1(12)$ transition at 6623.32 cm^{-1}, consisting of two transitions due to spin-rotation splitting, and the ${}^{q}P_2(10)$ transition at 6623.57 cm^{-1}, consisting of four transitions due to spin-rotation splitting. The transitions are labeled according to ${}^{\Delta K_a}\Delta J_{K''_a}(N'')$ where N is the rotational angular momentum quantum number, J is the sum of the rotational and spin angular momentum quantum numbers given by $N \pm {}^{1}/_{2}$, and K_a is the quantum number for rotation about the a axis of the molecule as defined in ref 26.

The ECDL was scanned with a sinusoidal ramp of 1.8 V peak-to-peak amplitude at a frequency of 0.532 Hz, giving a scan range of 12 GHz. Figure 9 shows the *fm*-NICE-OHMS spectra of HO_2 at 6623.32 and 6623.57 cm^{-1}, with peak absorption cross sections of $\sigma = 9.7 \times 10^{-20}$ cm^2 and $\sigma = 1.3 \times 10^{-19}$ cm^2, respectively.[35] In the case of HO_2, we were able to subtract a background measurement by just turning off the UV lamps, which resulted in a HO_2-free background after 10 s. No absorption features due to methanol were observed in the spectral range, but the effect of etalons within the setup on the spectra is clearly visible. A fit to the 6623.32 cm^{-1} absorption feature is shown in red in Figure 9a, but indicates a problem. With the Gaussian width constrained to the Doppler-broadened value [426 MHz (fwhm)], the returned Lorentzian component is close to zero, implying no substantial pressure broadening at 40 Torr of Ar. Thiebaud et al.[35] measured a fwhm for this transition as 660 MHz at 50 Torr He, and we would expect at least a similar pressure-broadening contribution under our conditions. The HO_2 measurements were taken toward the end of this study, when the diode laser was starting to exhibit multimode behavior, and the calibrated frequency scale (obtained from the spectrum analyzer traces) might be inaccurate. Although the results discussed above and taken

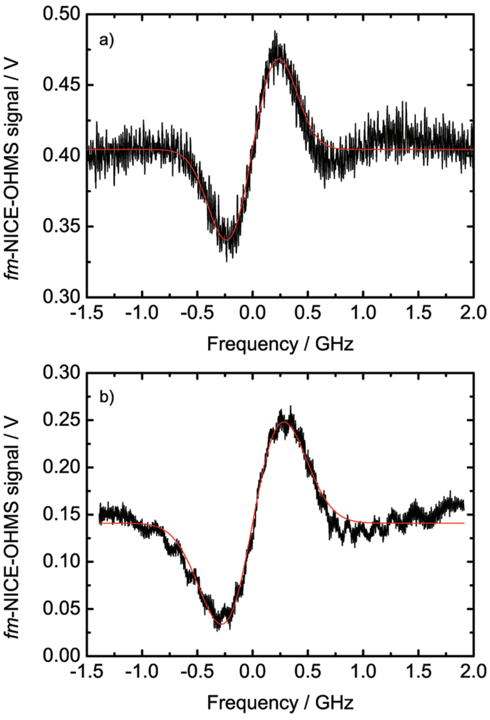

Figure 9. *fm*-NICE-OHMS spectra of HO_2 on the (a) $^{q}P_1(12)$ transition at 6623.32 cm^{-1} and (b) $^{q}P_2(10)$ transition at 6623.57 cm^{-1}, each with a fit to the data shown in red.

earlier in the study for other molecules returned sensible linewidths and pressure-broadening parameters, we concluded that our frequency calibration might be in error for the HO_2 measurements. For the $^{q}P_2(10)$ transition at 6623.57 cm^{-1}, a greater linewidth [Gaussian component of 576 ± 15 MHz (fwhm)] was obtained (Figure 9b), appearing to show the effects of the unresolved spin-rotation splitting. The ratio of linewidths of these two features, 1.36, is very similar to that found by Thiebaud et al. (1.35) and would be consistent with our present results showing the effect of an incorrect frequency scale.

Table 1 shows that formaldehyde is a stable photolysis product and that it absorbs weakly in the 6623 cm^{-1} range. A spectrum of pure H_2CO (50 mTorr) showed absorption features that did not coincide with those in Figure 9 but that would be observed in the frequency range scanned if the concentration was above the measured H_2CO detection limit of 6×10^{13} cm^{-3}. Modeling using the purely gas-phase kinetic scheme of Table 1 predicted the concentration of H_2CO to be 2×10^{14} cm^{-3}, a concentration that should have been observable. The absence of such absorption features suggests that the modeled concentration is too high, and inclusion of a wall-loss term[58] was found to decrease the concentration below the detection limit for values of the sticking coefficient above 10^{-5}. Formaldehyde is known to interact strongly with surfaces,[66] and values of $>10^{-5}$ are to be expected.

The data were calibrated against a known concentration of CH_4 in the same spectral range and taken at a similar time to the HO_2 measurement. The methane transition chosen was at 6623.19 cm^{-1}, with a peak absorption cross section of 1.69×10^{-23} cm^2 under Doppler-broadened conditions. With both data sets being taken at the same phase (absorption), the relative heights of the signals and the peak absorption cross sections were compared for the calibration. We note that we used a peak cross section for HO_2 obtained for 50 Torr of He,[35] and this might change somewhat for 40 Torr of Ar. The concentration of HO_2 was determined to be 6×10^{11} cm^{-3}, close to the expected value for HO_2 of 5.8×10^{11} cm^{-3} based on the simulations. Using this calibrated HO_2 concentration and the signal-to-noise ratio of 38 gave a minimum detection sensitivity of 1.8×10^{-9} cm^{-1}, and a minimum detectable concentration of ∼4×10^{10} radicals cm^{-3} is inferred. Comparing this value with those given in the Introduction, it can be seen that the sensitivity reported here is an order of magnitude lower than those reported for *fm*-NICE-OHMS previously. These measurements were conducted toward the end of the lifetime of the laser source, which was suffering degradation from repeated modulation over several years. In addition, the setup was also not working under optimal conditions, as one of the piezoelectric transducers received an erroneously large voltage that reduced its performance and meant that no *wm*-NICE-OHMS could be performed at this stage.

As a further confirmation that the species produced and detected from the photolysis experiments in the cavity was HO_2, two kinetic analyses were undertaken. Analysis of the time taken for the HO_2 signal to disappear following the cessation of the chlorine flow and analysis of the time taken for the HO_2 signal to disappear following switch-off of the UV lamps were investigated. The input flow rates for the flow controllers were set so that the residence time in the cavity was 120 s. Once all of the flows were on and the laser was locked and stable with *fm*-NICE-OHMS data being collected on HO_2, the chlorine flow was ceased. As the lamps remained on during this time, the photolysis reaction of Cl_2 continued, and it is this reaction that drove the formation of HO_2 until all of the Cl_2 was used or pumped away. The laser remained locked, with all of the other flows on, and data from scans over the same HO_2 $^{q}P_1(12)$ transition at 6623.32 cm^{-1} were recorded at approximately 20-s intervals. These data are shown in Figure 10 and have been offset in the *y* direction for clarity. It can be seen from the data that, over the 120 s following the cessation of the chlorine flow, the concentration of HO_2 dropped steadily as the remaining chlorine in the cavity was pumped out.

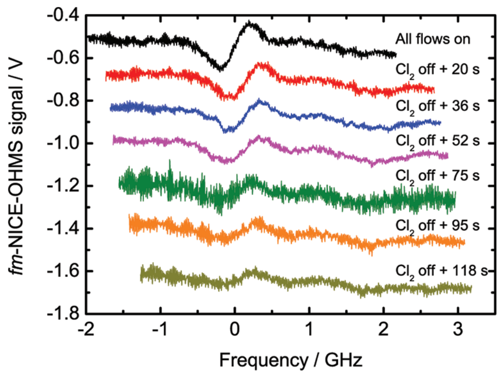

Figure 10. *fm*-NICE-OHMS data recorded over 2 min following the cessation of chlorine flow (data offset in the *y* direction for clarity).

The measurement of the decay of the HO_2 absorption feature after the lamps were switched off is shown in Figure 11. Error bars are shown in the figure; however, the error bars are small and so cannot be clearly seen. Also shown are two simulations of the decay starting from a HO_2 concentration of 5×10^{11} cm^{-3}: one from the kinetic scheme shown in Table 1

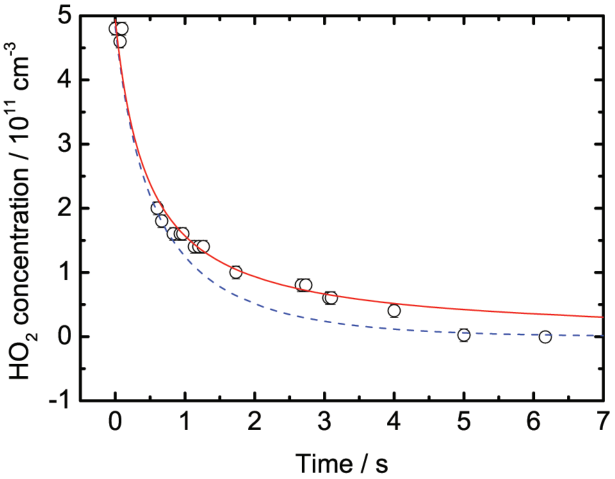

Figure 11. HO_2 concentration versus time after the UV lamps were turned off, together with the modeled HO_2 concentrations under two conditions, namely, with (dotted blue line) and without (solid red line) a wall-loss term (see text).

and one including the maximum possible wall-loss rate (when diffusion to the walls is the rate-limiting step and wall-loss coefficients are relatively high). Although the simulation without wall loss provides a better fit, it is clear that the simulations are in good agreement with the experimental data.

CONCLUSIONS AND OUTLOOK

This work has demonstrated the use of an external-cavity diode-laser-based NICE-OHMS system and its application to detection of a range of species of atmospheric importance. The spectrometer was successfully used to make the first measurements of the HO_2 radical species in a laboratory setting, marking a first step in applying this ultrasensitive spectrometer to real atmospheric scenarios. One of the key features of any detection technique is that it yields a direct and speciated solution. It has been demonstrated that the NICE-OHMS spectrometer can provide this for HO_2.

The experimental sensitivity limit achieved for detection of HO_2 was 1.8×10^{-9} cm^{-1} corresponding to $\sim 4 \times 10^{10}$ radicals cm^{-3}, which is not sufficiently sensitive to achieve detection of atmospheric levels. There is significant and real potential that these limits can be met with reasonably attainable improvements to the experimental system. In the current setup, there are two main limitations: the laser source and the mirrors. With improvements to the laser source to return the system to its optimal operating conditions, NICE-OHMS offers a viable, speciated, and compact spectrometer for application to atmospheric remote sensing. Although having a broad range, with a tunable ECDL allowing greater flexibility in the selection of the detection wavelength, the relatively large linewidth (2 MHz) of the laser locking system adds a further level of experimental complexity to the system, and maintaining the lock of the laser to the cavity during the wavelength scanning for data acquisition is difficult. With the implementation of an improved laser source, such as an erbium-doped fiber laser (EDFL), this situation would be improved, as the much narrower linewidth of the laser would allow it to be locked more easily to the cavity. In combination with fiber-coupled EOMs, this could lead to a compact and mobile fiber-based NICE-OHMS system. In a recent work, it was shown that the background signals originating from an imbalance of the phase-modulated triplet can be minimized by using appropriate types of EOMs.[49] Furthermore, it was shown that using an EOM with active feedback significantly reduces drifts and noise in the system, as was also previously shown by Bell et al.[50] Higher powers would also improve the signal size with an associated reduction in the shot-noise limit for the setup. The current sensitivity was achieved with a cavity of relatively low finesse, which could be improved by the use of higher-reflectivity mirrors; it should be noted, however, that this will change the locking response of the cavity. Although the implementation of a narrow-linewidth EDFL would increase the ease of locking, the spectral coverage limitations of such laser sources might hamper the application of such a laser in the atmospheric-pressure-broadened regime.

AUTHOR INFORMATION

Corresponding Author

*E-mail: grant.ritchie@chem.ox.ac.uk. Phone: +44 (0)1865 285723. Fax: +44 (0)1865 275410.

Notes

The authors declare no competing financial interest.

ACKNOWLEDGMENTS

This work was conducted under the EPSRC Programme Grant EP/E019765/1: New frontiers in quantitative infra-red to ultraviolet spectroscopy using diode and quantum cascade lasers. The authors gratefully acknowledge the New Zealand Foundation for Research, Science and Technology (Contract UOXX0501) for supporting N.J.v.L. C.L.B. is grateful to the NERC for a studentship. We are particularly grateful to a reviewer for making most helpful suggestions and improvements to this article.

REFERENCES

(1) Heard, D. E. *Annu. Rev. Phys. Chem.* **2006**, *57*, 191−216.

(2) Heard, D. E.; Pilling, M. J. *Chem. Rev.* **2003**, *103*, 5163−5198.

(3) Clemitshaw, K. C. *Crit. Rev. Environ. Sci. Technol.* **2004**, *34*, 1−108.

(4) Heard, D. E. Stratospheric chemistry and composition: Hydroxyl radical. In *Encyclopedia of Atmospheric Sciences*; Holton, J. R., Pyle, J. A., Curry, J. A., Eds.; Elsevier: Amsterdam, 2003; pp 2185−2193.

(5) Monks, P. S. *Chem. Soc. Rev.* **2005**, *34*, 376−395.

(6) Parra, J.; George, L. A. *Appl. Opt.* **2009**, *48*, 3355−3361.

(7) Dusanter, S.; Vimal, D.; Stevens, P. S.; Volkamer, R.; Molina, L. T. *Atmos. Chem. Phys.* **2009**, *9*, 1665−1685.

(8) Whalley, L. K.; Furneaux, K. L.; Goddard, A.; Lee, J. D.; Mahajan, A.; Oetjen, H.; Read, K. A.; Kaaden, N.; Carpenter, L. J.; Lewis, A. C.; Plane, J. M. C.; Saltzman, E. S.; Wiedensohler, A.; Heard, D. E. *Atmos. Chem. Phys.* **2010**, *10*, 1555−1576.

(9) Cantrell, C. A.; Stedman, D. H.; Wendel, G. J. *Anal. Chem.* **1984**, *56*, 1496−1502.

(10) Wood, E. C.; Cohen, R. C. Fluorescence Methods. In *Analytical Techniques for Atmospheric Measurement*; Heard, D. E., Ed.; Blackwell Publishing: Oxford, U.K., 2006; Chapter 4, pp 189−228.

(11) Clemitshaw, K. C.; Carpenter, L. J.; Penkett, S. A.; Jenkin, M. E. *J. Geophys. Res.* **1997**, *102*, 25405−25416.

(12) Green, T. J.; Reeves, C. E.; Brough, N.; Edwards, G. D.; Monks, P. S.; Penkett, S. A. *J. Environ. Monit.* **2003**, *5*, 75−83.

(13) Liu, Y.; Morales-Cueto, R.; Hargrove, J.; Medina, D.; Zhang, J. *Environ. Sci. Technol.* **2009**, *43*, 7791−7796.

(14) Fuchs, H.; Bohn, B.; Hofzumahaus, A.; Holland, F.; Lu, K. D.; Nehr, S.; Rohrer, F.; Wahner, A. *Atmos. Meas. Tech.* **2011**, *4*, 1209−1225.

(15) Miyazaki, K.; Parker, A. E.; Fittschen, C.; Monks, P. S.; Kajii, Y. *Atmos. Meas. Tech.* **2010**, *3*, 1547−1554.

(16) Jenkin, M. E.; Cox, R. A.; Hayman, G. D.; Whyte, L. J. *J. Chem. Soc., Faraday Trans. 2* **1988**, *84*, 913–930.

(17) Crowley, J. N.; Simon, F. G.; Burrows, J. P.; Moortgat, G. K.; Jenkin, M. E.; Cox, R. A. *J. Photochem. Photobiol. A* **1991**, *60*, 1–10.

(18) Jemi-Alade, A. A.; Lightfoot, P. D.; Lesclaux, R. *Chem. Phys. Lett.* **1992**, *195*, 25–30.

(19) Tomas, A.; Villenave, E.; Lesclaux, R. *J. Phys. Chem. A* **2001**, *105*, 3505–3514.

(20) Nielsen, O. J.; Johnson, M. S.; Wallington, T. J.; Christensen, L. K.; Platz, J. *Int. J. Chem. Kinet.* **2002**, *34*, 283–291.

(21) Christensen, L. E.; Okumura, M.; Sander, S. P.; Salawitch, R. J.; Toon, G. C.; Sen, B.; Blavier, J. F.; Jucks, K. W. *Geophys. Res. Lett.* **2002**, *29*, 1299.

(22) Stone, D.; Rowley, D. M. *Phys. Chem. Chem. Phys.* **2005**, *7*, 2156–2163.

(23) Johnson, T. J.; Wienhold, F. G.; Burrows, J. P.; Harris, G. W.; Burkhard, H. *J. Phys. Chem.* **1991**, *95*, 6499–6502.

(24) Fink, E. H.; Ramsay, D. A. *J. Mol. Spectrosc.* **1997**, *185*, 304–324.

(25) Taatjes, C. A.; Oh, D. B. *Appl. Opt.* **1997**, *36*, 5817–5821.

(26) DeSain, J. D.; Hob, A. D.; Taatjesb, C. A. *J. Mol. Spectrosc.* **2003**, *219*, 163–169.

(27) Christensen, L. E.; Okumura, M.; Sander, S. P.; Friedl, R. R.; Miller, C. E.; Sloan, J. J. *J. Phys. Chem.* **2004**, *108*, 80–91.

(28) Kanno, N.; Tonokura, K.; Tezaki, A.; Koshi, M. *J. Phys. Chem. A* **2005**, *109*, 3153–3158.

(29) Kanno, N.; Tonokura, K.; Tezaki, A.; Koshi, M. *J. Mol. Spectrosc.* **2005**, *229*, 193–197.

(30) Christensen, L. E.; Okumura, M.; Hansen, J. C.; Sander, S. P.; Francisco, J. S. *J. Phys. Chem. A* **2006**, *110*, 6948–6959.

(31) Taatjes, C. A. *J. Phys. Chem. A* **2006**, *110*, 4299–4312.

(32) Thiebaud, J.; Fittschen, C. *Appl. Phys. B: Lasers Opt.* **2006**, *85*, 383–389.

(33) Suzaki, K.; Kanno, N.; Tonokura, K.; Koshi, M.; Tsuchiya, K.; Tezaki, A. *Chem. Phys. Lett.* **2006**, *425*, 179–184.

(34) Ibrahim, N.; Thiebaud, J.; Orphal, J; Fittschen, C. *J. Mol. Spectrosc.* **2007**, *242*, 64–69.

(35) Thiebaud, J.; Crunaire, S.; Fittschen, C. *J. Phys. Chem. A* **2007**, *111*, 6959–6966.

(36) Aluculesei, A.; Tomas, A.; Schoemaecker, C.; Fittschen, C. *Appl. Phys. B: Lasers Opt.* **2008**, *92*, 379–385.

(37) Tang, Y.; Tyndall, G. S.; Orlando, J. J. *J. Phys. Chem. A* **2010**, *114*, 369–378.

(38) Zahniser, M. S.; Stanton, A. C. *J. Chem. Phys.* **1984**, *80*, 4951–4960.

(39) Zahniser, M. S.; McCurdy, K. E.; Stanton, A. C. *J. Phys. Chem.* **1989**, *93*, 1065–1070.

(40) Miyano, S.; Tonokura, K. *J. Mol. Spectrosc.* **2011**, *265*, 47–51.

(41) Sakamoto, Y.; Tonokura, K. *J. Phys. Chem. A* **2012**, *116*, 215–222.

(42) Thiebaud, J.; Parker, A.; Fittschen, C.; Vincent, G.; Zahraa, O.; Marquaire, P.-M. *J. Phys. Chem. C* **2008**, *112*, 2239–2243.

(43) van Helden, J. H.; Peverall, R.; Ritchie, G. A. D. Cavity enhanced techniques using continuous wave lasers. In *Cavity Ring-Down Spectroscopy: Techniques and Applications*; Engeln, R.; Berden, G., Eds; Wiley-Blackwell: Oxford, U.K., 2009; Chapter 2, pp 27–56.

(44) Ye, J.; Ma, L.-S.; Hall, J. L. *J. Opt. Soc. Am. B* **1998**, *15*, 6–15.

(45) Ma, L.-S.; Ye, J.; Dube, P.; Hall, J. L. *J. Opt. Soc. Am. B* **1999**, *16*, 2255–2268.

(46) van Leeuwen, N. J.; Wilson, A. C. *J. Opt. Soc. Am. B* **2004**, *21*, 1713–1721.

(47) Schmidt, F.; Foltynowicz, A.; Ma, W.; Lock, T.; Axner, O. *Opt. Express* **2007**, *15*, 10822–10831.

(48) Foltynowicz, A.; Wang, J.; Ehlers, P.; Axner, O. *Opt. Express* **2010**, *18*, 18580–18591.

(49) Foltynowicz, A.; Silander, I.; Axner, O. *J. Opt. Soc. Am. B* **2011**, *28*, 2797–2805.

(50) Bell, C. L.; Hancock, G.; Peverall, R.; Ritchie, G. A. D.; van Helden, J. H.; van Leeuwen, N. J. *Opt. Express* **2009**, *17*, 9834–9839.

(51) Drever, R. W. P.; Hall, J. L. H.; Kowalski, F. V.; Hough, J.; Ford, G. M.; Munley, A. J.; Ward, H. *Appl. Phys. B: Lasers Opt.* **1983**, *31*, 97–105.

(52) DeVoe, R. G.; Brewer, R. G. *Phys. Rev. A: At., Mol., Opt. Phys.* **1984**, *30*, 2827–2829.

(53) Sander, S. P.; Abbatt, J.; Barker, J. R.; Burkholder, J. B.; Friedl, R. R.; Golden, D. M.; Huie, R. E., Kolb, C. E., Kurylo, M. J.; Moortgat, G. K.; Orkin, V. L.; Wine, P. H. *Chemical Kinetics and Photochemical Data for Use in Atmospheric Studies, Evaluation No. 17*; JPL Publication 10-6; Jet Propulsion Laboratory: Pasadena, CA, 2011; available at http://jpldataeval.jpl.nasa.gov.

(54) Tsang, W. J. *J. Phys. Chem. Ref. Data* **1987**, *16*, 471–508.

(55) Pagsberg, P.; Munk, J.; Sillesen, A.; Anastasi, C. *Chem. Phys. Lett.* **1988**, *146*, 375–381.

(56) Tyndall, G. S.; Orlando, J. J.; Kegley-Owen, C. S.; Wallington, T. J.; Hurley, M. D. *Int. J. Chem. Kinet.* **1999**, *31*, 776–784.

(57) Burrows, J. P.; Tyndall, G. S.; Moortgat, G. K. *J. Phys. Chem.* **1985**, *89*, 4848–4856.

(58) Chantry, P. J. *J. Appl. Phys.* **1987**, *62*, 1141–1148.

(59) Rothman, L. S.; Jacquemart, D.; Barbe, A.; Benner, D. C.; Birk, M.; Brown, L. R.; Carleer, M. R.; Chackerian, C., Jr.; Chance, K.; Coudert, L. H.; Dana, V.; Devi, V. M.; Flaud, J.-M.; Gamache, R. R.; Goldman, A.; Hartmann, J.-M.; Jucks, K. W.; Maki, A. G.; Mandin, J.-Y.; Massie, S. T.; Orphal, J.; Perrin, A.; Rinsland, C. P.; Smith, M. A. H.; Tennyson, J.; Tolchenov, R. N.; Toth, R. A.; Vander Auwera, J.; Varanasi, P.; Wagner, G. *J. Quant. Spectrosc. Radiat. Transfer* **2005**, *96*, 139–204.

(60) Campargue, A.; Wang, L.; Liu, A. W.; Hu, S. M.; Kassi, S. *Chem. Phys.* **2010**, *373*, 203–210.

(61) Predoi-Cross, A.; Brown, L. R.; Malathy Devi, V.; Brawley-Tremblay, M.; Chris Benner, D. *J. Mol. Spectrosc.* **2005**, *232*, 231–246.

(62) Smith, M. A. H.; Chris Benner, D.; Predoi-Cross, A.; Malathy Devi, V. *J. Quant. Spectrosc. Radiat. Transfer* **2010**, *111*, 1152–1166.

(63) Zéninari, V.; Parvitte, B.; Courtois, D.; Kapitanov, V. A.; Ponomarev, Yu. N. *Appl. Phys. B: Lasers Opt.* **2001**, *72*, 953–959.

(64) Yamano, D.; Sakamato, Y.; Yabushita, A.; Kawasaki, M.; Morino, I.; Inoue, G. *Appl. Phys. B: Lasers Opt.* **2009**, *97*, 523–528.

(65) Nakayama, T.; Fukuda, H.; Sugita, A.; Hashimoto, S.; Kawasaki, M.; Aloisio, S.; Morino, I.; Inoue, G. *Chem. Phys.* **2007**, *334*, 196–203.

(66) Dahnke, H.; Von Basum, G.; Kleinermanns, K.; Hering, P.; Mürtz, M. *Appl. Phys. B: Lasers Opt.* **2002**, *75*, 311–316.